

ARMY RESEARCH LABORATORY



**Macro-magnetic Modeling of the ARL
Microelectromechanical System (MEMS) Flux Concentrator**

by Gregory A. Fischer and Alan S. Edelstein

ARL-TR-5778

September 2011

NOTICES

Disclaimers

The findings in this report are not to be construed as an official Department of the Army position unless so designated by other authorized documents.

Citation of manufacturer's or trade names does not constitute an official endorsement or approval of the use thereof.

Destroy this report when it is no longer needed. Do not return it to the originator.

Army Research Laboratory

Adelphi, MD 20783-1197

ARL-TR-5778

September 2011

**Macro-magnetic Modeling of the ARL
Microelectromechanical System (MEMS) Flux Concentrator**

**Gregory A. Fischer and Alan S. Edelstein
Sensors and Electron Devices Directorate, ARL**

Approved for public release; distribution unlimited.

REPORT DOCUMENTATION PAGE

Form Approved
OMB No. 0704-0188

Public reporting burden for this collection of information is estimated to average 1 hour per response, including the time for reviewing instructions, searching existing data sources, gathering and maintaining the data needed, and completing and reviewing the collection information. Send comments regarding this burden estimate or any other aspect of this collection of information, including suggestions for reducing the burden, to Department of Defense, Washington Headquarters Services, Directorate for Information Operations and Reports (0704-0188), 1215 Jefferson Davis Highway, Suite 1204, Arlington, VA 22202-4302. Respondents should be aware that notwithstanding any other provision of law, no person shall be subject to any penalty for failing to comply with a collection of information if it does not display a currently valid OMB control number.

PLEASE DO NOT RETURN YOUR FORM TO THE ABOVE ADDRESS.

1. REPORT DATE (DD-MM-YYYY) September 2011		2. REPORT TYPE Final		3. DATES COVERED (From - To) 2003–2011	
4. TITLE AND SUBTITLE Macro-magnetic Modeling of the ARL MEMS Flux Concentrator				5a. CONTRACT NUMBER	
				5b. GRANT NUMBER	
				5c. PROGRAM ELEMENT NUMBER	
6. AUTHOR(S) Gregory A. Fischer and Alan S. Edelstein				5d. PROJECT NUMBER	
				5e. TASK NUMBER	
				5f. WORK UNIT NUMBER	
7. PERFORMING ORGANIZATION NAME(S) AND ADDRESS(ES) U.S. Army Research Laboratory ATTN: RDRL-SES-P 2800 Powder Mill Road Adelphi, MD 20783-1197				8. PERFORMING ORGANIZATION REPORT NUMBER ARL-TR-5778	
9. SPONSORING/MONITORING AGENCY NAME(S) AND ADDRESS(ES)				10. SPONSOR/MONITOR'S ACRONYM(S)	
				11. SPONSOR/MONITOR'S REPORT NUMBER(S)	
12. DISTRIBUTION/AVAILABILITY STATEMENT Approved for public release; distribution unlimited.					
13. SUPPLEMENTARY NOTES					
14. ABSTRACT Magnetic flux concentrators are soft magnetic materials typically used to focus magnetic field lines in an effort to increase the sensitivity of a magnetic sensor. The use of magnetoresistive sensors, especially given the recent development of magnetic tunnel junctions (MTJ) with magnesium oxide (MgO) barriers exhibiting magnetoresistance values as large as 400%, has created interest in flux concentrators as an avenue to not only increase sensitivity but also mitigate the 1/f noise that is prevalent in these devices at low frequencies. Here we describe the magnetic modeling performed at the U.S. Army Research Laboratory (ARL) that has facilitated the development of the microelectromechanical system (MEMS) flux concentrator, a device that uses magnetic flux concentrators deposited on MEMS structures that modulate low frequency signals at the position of the sensor, essentially shifting the signal of interest to a frequency range in which 1/f noise is much lower. We present magnetic modeling results of various designs, including our current design, focusing on key design elements.					
15. SUBJECT TERMS Magnetic flux, flux concentrator, magnetic modeling					
16. SECURITY CLASSIFICATION OF:			17. LIMITATION OF ABSTRACT UU	18. NUMBER OF PAGES 24	19a. NAME OF RESPONSIBLE PERSON Gregory A. Fischer
a. REPORT Unclassified	b. ABSTRACT Unclassified	c. THIS PAGE Unclassified			19b. TELEPHONE NUMBER (Include area code) (301) 394-2089

Contents

List of Figures	iv
List of Tables	iv
1. Introduction	1
2. Concept of the MEMS Flux Concentrator	1
3. Magnetic Modeling Details and Parameters	2
3.1 Pivoting Flux Concentrators.....	4
3.2 Comb Drive, Out-of-phase Flux Concentrators	6
3.3 Comb Drive, In-phase Flux Concentrators.....	9
4. Discussion and Conclusions	12
5. References	14
List of Symbols, Abbreviations, and Acronyms	16
Distribution List	17

List of Figures

Figure 1. (a) Magnetoresistance of a spin valve with small and larger flux concentrators and (b) an enlarged view of the data near zero applied field.	3
Figure 2. Schematic of the rotating MEMS flux concentrator. All dimensions are in microns.	5
Figure 3. Magnetic field enhancement at the center of the air gap when the flaps are in the plane of the sensor position.	5
Figure 4. Enhancement of the magnetic field at the position of the magnetic sensor as a function of tilt angle of the MEMS flaps for various air gap sizes.	6
Figure 5. Enhancement curves generated from models of permalloy flux concentrator pairs with and without release holes.	7
Figure 6. Modulation as a function of the motion of the flux concentrator flaps.	8
Figure 7. Enhancement curves demonstrating effect of the addition of a second pair of large, stationary flux concentrators.	9
Figure 8. (a) Optical microscope image of the in-phase flux concentrator design and (b) the concentrators as drawn for modeling. The darker trapazoids are part of the stationary concentrators, the remainder being out of view.	10
Figure 9. (a) Top view and (b) side view of magnetic flux lines around concentrators. Color from blue to red denotes low to high flux density, respectively.	11
Figure 10. Flow of magnetic flux lines around etch holes in concentrators.	11
Figure 11. Variations in the magnetic field strength at 1 micron above concentrators due to etch holes.	12
Figure 12. Four MEMs flux concentrator devices packaged for testing.	13

List of Tables

Table 1. Enhancements provided by flux concentrators.	4
--	---

1. Introduction

Magnetically soft (high permeability) materials are often used as magnetic field concentrators in magnetic sensor systems. These magnetic flux concentrators improve the sensitivity of the associated system by increasing the magnetic flux at the position of the sensor. Flux concentrators have been used with spin valves (1), hall sensors (2), atomic magnetometers (3), superconducting quantum interference devices (SQUIDs) (4), resonating magnetic sensors (5), and magnetic tunnel junctions (6). The concentration effect is a function of (1) the relative permeability (μ_r) of the material used to make the flux concentrators, (2) the area ratio between the ends of a concentrator (7), and (3) the size of the air gap between adjacent flux concentrators (8). It has been shown that, with judicious choices of flux concentrator geometry and air gap size, magnetic field amplification can exceed the theoretical value fixed by μ_r of the material used (7).

Magnetoresistive (MR) devices, particularly magnetic tunnel junctions (MTJs), are excellent candidates for low-cost, low-power magnetic sensors. While MTJs can provide excellent detectivity, taking full advantage of these values at low frequencies ($f < 100$ Hz) requires finding a method of mitigating $1/f$ noise (9, 10). We have reported elsewhere (11) on the successful fabrication and validation of a concept for mitigating the effect of $1/f$ noise by increasing the operating frequency of the magnetic sensor to a region where $1/f$ noise is much smaller. The idea is to place the magnetic sensor between flux concentrators that have been deposited on microelectromechanical system (MEMS) flaps. An essential part of designing the device was understanding the behavior of the magnetic field lines both for enhancing the field at the position of the sensor as well as maximizing modulation of the field. These needs motivated our work on macro-magnetic modeling.

2. Concept of the MEMS Flux Concentrator

The key concept of the MEMS flux concentrator is that the flux concentrators are set into oscillatory motion. Once set into periodic motion at frequencies of around 10 kHz or more, the enhancement of the magnetic field at the position of the sensor is modulated. Due to this high frequency modulation, the sensor operates at a frequency where the $1/f$ noise is much smaller. Sidebands to the drive signal and its first harmonic appear due to this modulation. There are at least two major matters that have to be addressed before the potential advantages of this device can be realized. First, it is necessary that the sensor element is responsible for most of the $1/f$ noise and not some other part of the sensor system. The second issue, the design and fabrication of the device, is discussed in the sections concerning specific designs.

As described here, the MEMS flux concentration will greatly reduce the $1/f$ noise of the magnetic sensors. It does nothing to reduce the $1/f$ noise of the flux concentrators themselves. Thus, if the concept is going to be useful, it is necessary that the $1/f$ noise of the flux concentrators be much less than the $1/f$ noise of the magnetic sensors. This requirement motivated a series of experiments to see if this requirement was fulfilled. As we reported elsewhere (12), the noise voltage of spin valves with and without adjacent, stationary flux concentrators are indistinguishable. This result implies that the $1/f$ of the flux concentrators is much less than the $1/f$ noise of the spin valves.

3. Magnetic Modeling Details and Parameters

We performed magnetic modeling using a commercial finite element code program called Maxwell 3D, from ANSYS. Maxwell 3D is capable of analyzing AC magnetic, DC magnetic, and electrostatic field problems. The three-dimensional (3-D) DC magnetic portion of the software computes static magnetic fields, where the source originates from a DC current or voltage, permanent magnets, or externally applied magnetic fields. It can directly compute the magnetic field (H) and current distribution (J), and derive the magnetic flux density (B) from the H field. In addition, it can automatically calculate force, torque, inductances, and saturation in devices containing linear, nonlinear, and anisotropic materials. The post-processor portion of the software can provide plots of flux lines, B and H fields, energy densities, and saturation. The modeling process consists of drawing the objects of interest, assigning properties (coercivity, permeability, etc.) to the objects, assigning boundaries or sources, seeding the objects and creating a mesh, and then the processing of the now defined problem.

Each model investigated involved the same fundamental sequence of steps. The first step in the analysis of the flux concentrator was to draw the model. Drawing the model consists of drawing 3-D objects and either joining them together or subtracting them from each other. This allows one to create complex objects. A sufficiently large region around the flux concentrators and sensing region was defined as a background. The flux concentrators are drawn as solid pieces and assigned the material properties of permalloy (nickel-iron [NiFe]) with a permeability of 5,000 as that is a value that is readily achieved in thin films of the material. The material properties assigned to this background are those of a vacuum, with a relative permeability of 1. The modeling is macro-magnetic in nature as it does not take into account domain structure but does incorporate demagnetization factors. The initial mesh is created by the program but one can create regions in which the initial mesh is denser so as to force more tetrahedrons into regions where one has a greater interest in the solutions without significantly increasing solution time. Mesh refinement is also handled by the program as part of an iterative process in which energy error and percentage decreases to a predetermined figure.

In order to determine the accuracy of the modeling results, measurements were made using spin valves and fixed flux concentrators. Two different sizes of trapezoidal-shaped flux concentrators were fabricated and measurements of the magnetoresistance were made for (1) only spin valves, (2) a spin valve between a pair of “normal” flux concentrators, and (3) a spin valve between a pair of larger flux concentrators. The smaller pair of flux concentrators had a height of 104 μm , a short side length of 80 μm , and a long side length of 150 μm . The larger pair of flux concentrators was 80 μm long on the short side and 300 μm long on the long side, and had a height of 315 μm . The air gap between both types of flux concentrators was held constant at 52 μm . Figure 1 shows the resistance of the spin valves with and without the flux concentrators. The amount that the flux concentrators enhanced the field was compared to calculated values from magnetic modeling and the results are shown in table 1, showing that the measured field enhancement provided by stationary flux concentrators agrees to within 4% of the values determined from the model results. These results are particularly good considering the flux concentrators were modeled as solid pieces of permalloy, while the actual samples consisted of two repeats of 40 \AA chromium (Cr)/1500 \AA permalloy.

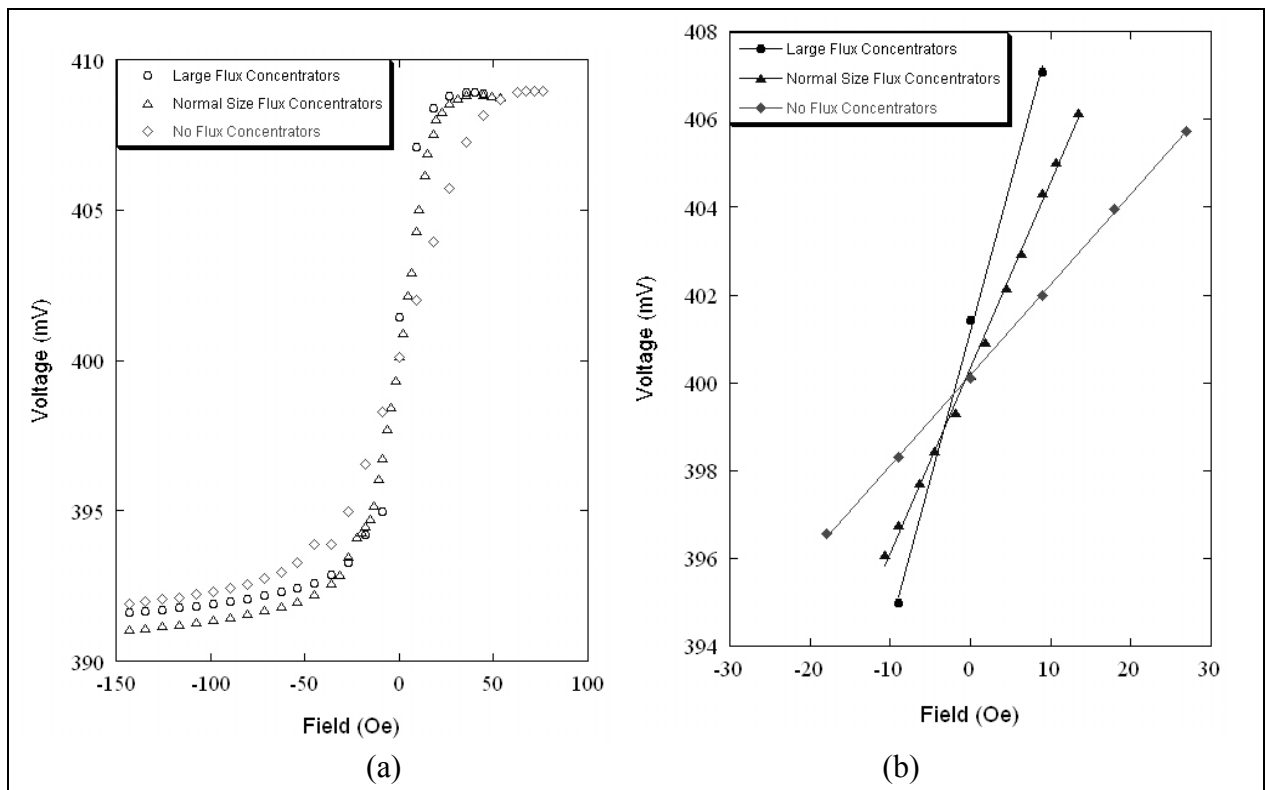


Figure 1. (a) Magnetoresistance of a spin valve with small and larger flux concentrators and (b) an enlarged view of the data near zero applied field.

Table 1. Enhancements provided by flux concentrators.

	Ave. Linear Region Slope (mV/Oe)*	Measured Enhancement	Calculated Enhancement
No Flux Concentrator	0.21133	–	–
Small Flux Concentrator	0.41826	1.98	1.93
Large Flux Concentrator	0.69586	3.29	3.36

*Voltage across spin valve was set to ~400 mV in all cases.

We are interested in the magnetic field strength and flux line behavior at the position the sensor would occupy. Two main quantities of interest to us are the enhancement factor and the percentage modulation. The enhancement factor E_H is defined as H_S/H_{appl} , where H_S and H_{appl} denote the magnetic field strength at the position the sensor would occupy and the magnetic field strength far from the concentrators, respectively. For the rotating flux concentrator design and the out of phase design, we define the percentage of modulation of the field at the position of the sensor as

$$[(H_{S2} - H_{S1})/H_{Sr}] * 100, \quad (1)$$

where H_{S2} and H_{S1} are the enhancement factors at the two end points of motion and H_{Sr} is the enhancement factor when the flux concentrators are at rest in their neutral position. Determining the modulation for the in-phase design is discussed in the corresponding section. The next sections discuss the three primary designs we have modeled.

3.1 Pivoting Flux Concentrators

The first design of the MEMS flux concentrator used electrostatic plates to drive the motion of the concentrators. The concentrators perform oscillatory rotation about the torsional suspensions (figure 2), thus modulating the field at the position of the sensor. Using the geometry of the “normal” concentrators flaps, described previously, and assuming both a 3- μm gap and 0.5- μm thickness of permalloy, we ran models to determine how the enhancement of the field at the center of the air gap would vary with permeability. One sees in figure 3 that for permeabilities near the values expected for permalloy (around 5000) the enhancement is a rather weak function of the permeability. Thus, it is not necessary to maximize the permeability. Holding the permeability constant we then looked at how rotation of the flaps alters the enhancement for various air gap sizes. For a given gap size, the model was run for each degree of tilt angle from 0° to 6°. The results are shown in figure 4 and one sees that a large modulation of the field can be achieved at the position of the sensor though the modulation decreases rapidly as the distance between the flaps is increased. Unfortunately, the processing necessary to liberate the flaps for

rotation consistently destroyed the magnetic sensor stack, regardless of what sort of protective coating was used. This necessitated a change in design.

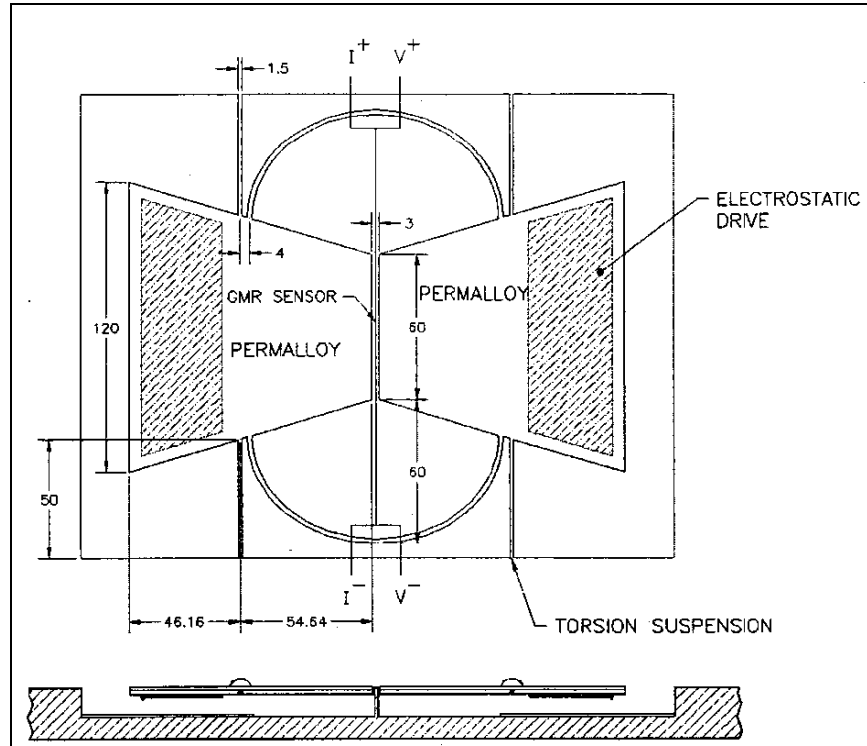


Figure 2. Schematic of the rotating MEMS flux concentrator. All dimensions are in microns.

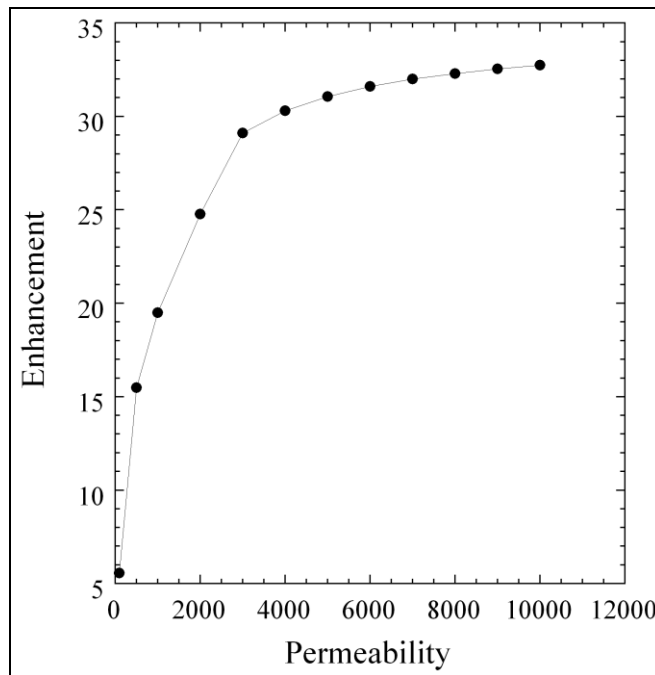


Figure 3. Magnetic field enhancement at the center of the air gap when the flaps are in the plane of the sensor position.

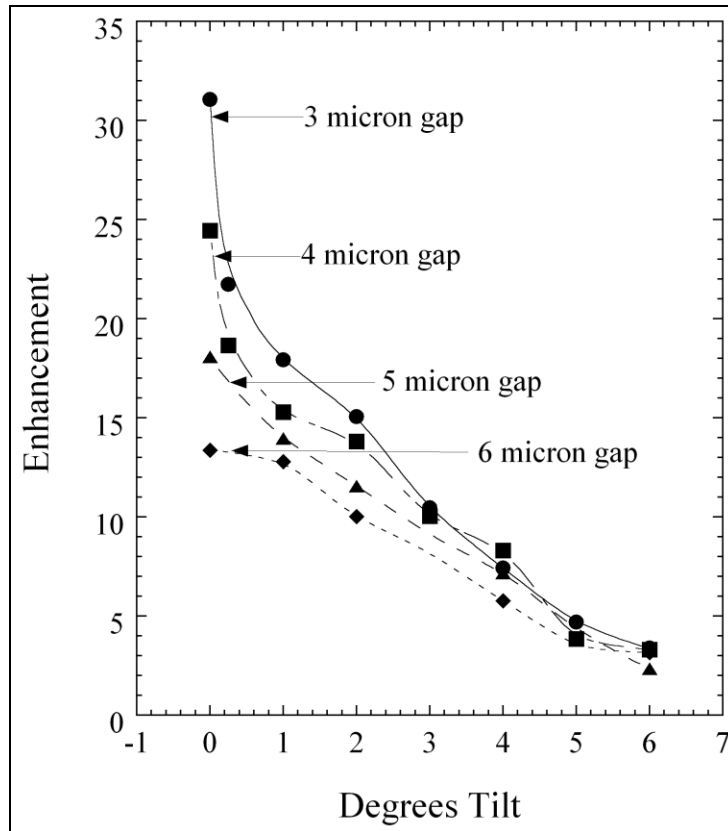


Figure 4. Enhancement of the magnetic field at the position of the magnetic sensor as a function of tilt angle of the MEMS flaps for various air gap sizes.

3.2 Comb Drive, Out-of-phase Flux Concentrators

To avoid damaging the magnetic sensors during the release step of fabricating the MEMS structure by exposing them to hydrofluoric acid (HF), two chips were used: one with the MEMS structure and the flux concentrators and the other with the magnetic sensors. The two chips were combined with flip chip bonding. The sensor chip was separated from the MEMS chip by about 4 μm . The MEMS spring widths were varied between 4 and 10 μm . The spin valves on the underneath side of the sensor chip are 12 μm wide. The two MEMS flaps on each side of the spin valve were connected by silicon springs so that the desired in plane, out-of-phase motion of the flaps was a normal mode. The MEMS flaps are driven to move at this normal mode by electrostatic comb drives. It was determined that for proper release of the concentrators, etch holes would need to be added to the flaps. Further details on this design have been previously published (11, 12).

Three different sets of magnetic modeling were performed for this version of the MEMS flux concentrator: (1) solid flaps, (2) flaps with slit shaped release holes, and (3) flaps with squareshaped release holes. In all of these models, the field values were determined at the new

position of the sensor, 4 μm above the plane of the flaps. The flaps were modeled as solid permalloy and all nonmagnetic structural material was ignored. The magnetic material of the spin valve was also ignored as the thicknesses of the various layers are small enough to have only a small influence on the surrounding flux environment. Enhancement curves for each case are created from the results of running models for various air gap sizes (figure 5). The out-of-phase motion causes the air gap to decrease (increase) as the flaps move towards (away) from each other. The enhancement curve is used to determine the percentage field modulation at the position of the sensor based on how far the flaps move. Equation 1 and the results of the models for the square etch holes were used to create a modulation curve (figure 6). From the modulation curve, we were able to determine that achieving 50% modulation of the magnetic field at the position of the sensor would require 38 μm of total travel or $\pm 19 \mu\text{m}$ of motion of the flux concentrators.

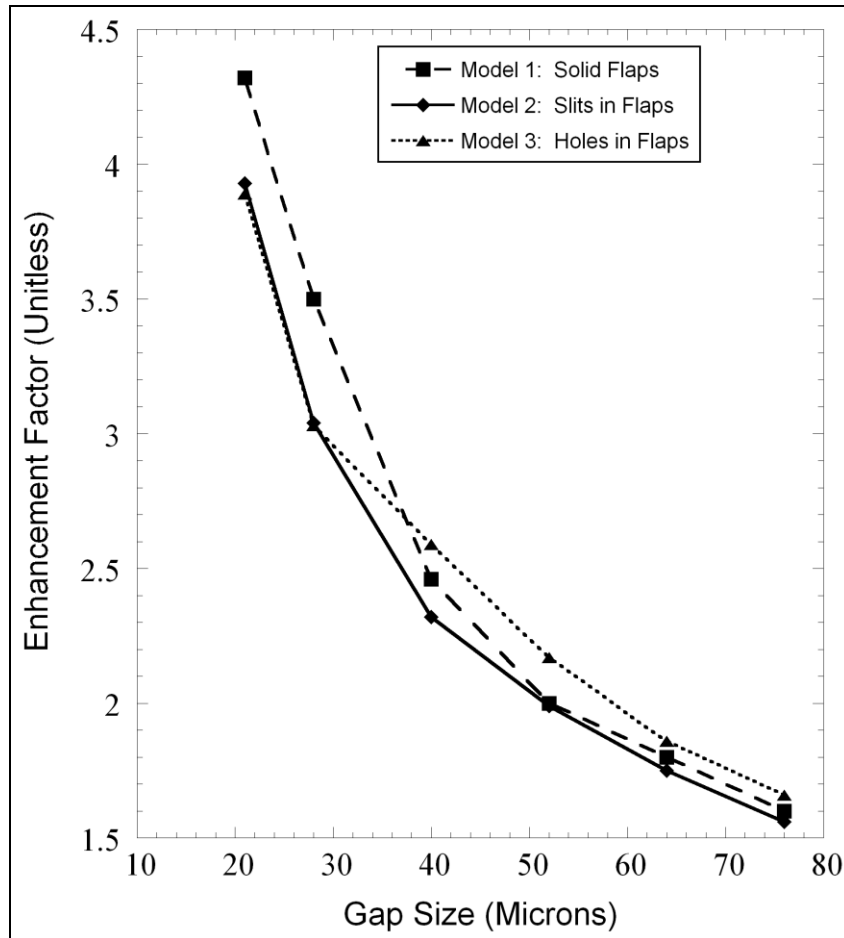


Figure 5. Enhancement curves generated from models of permalloy flux concentrator pairs with and without release holes.

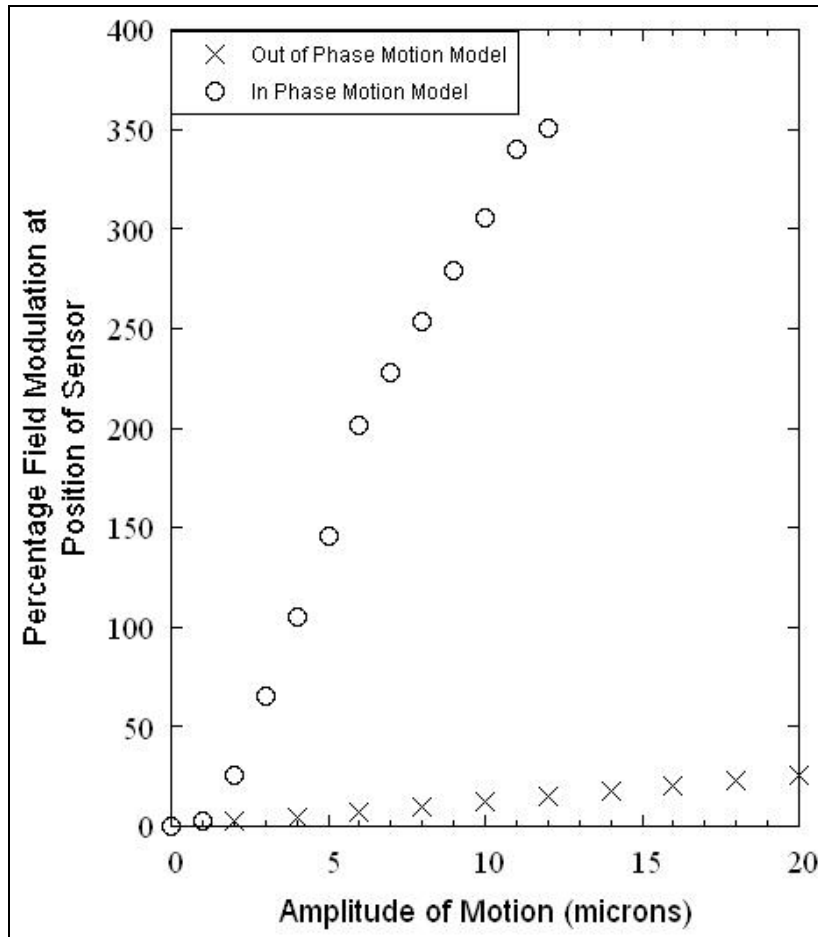


Figure 6. Modulation as a function of the motion of the flux concentrator flaps.

In an effort to increase not only the enhancement of the field at the position of the sensor but also increase the modulation beyond a factor of 2 without needing 19 μm of motion, we modeled the addition of a second pair of larger, stationary flux concentrators. These stationary flaps were to be on the wafer containing the sensor and were drawn to have a height of 2000 μm , a short side length of 125 μm , and a long side length of 150 μm . The thickness of the permalloy for these concentrators was set at 0.5 μm and they had a 50% overlap of the moving concentrators. As shown in figure 7, the field enhancement at the position of the sensor was indeed increased but the modulation was still roughly a factor of 2.

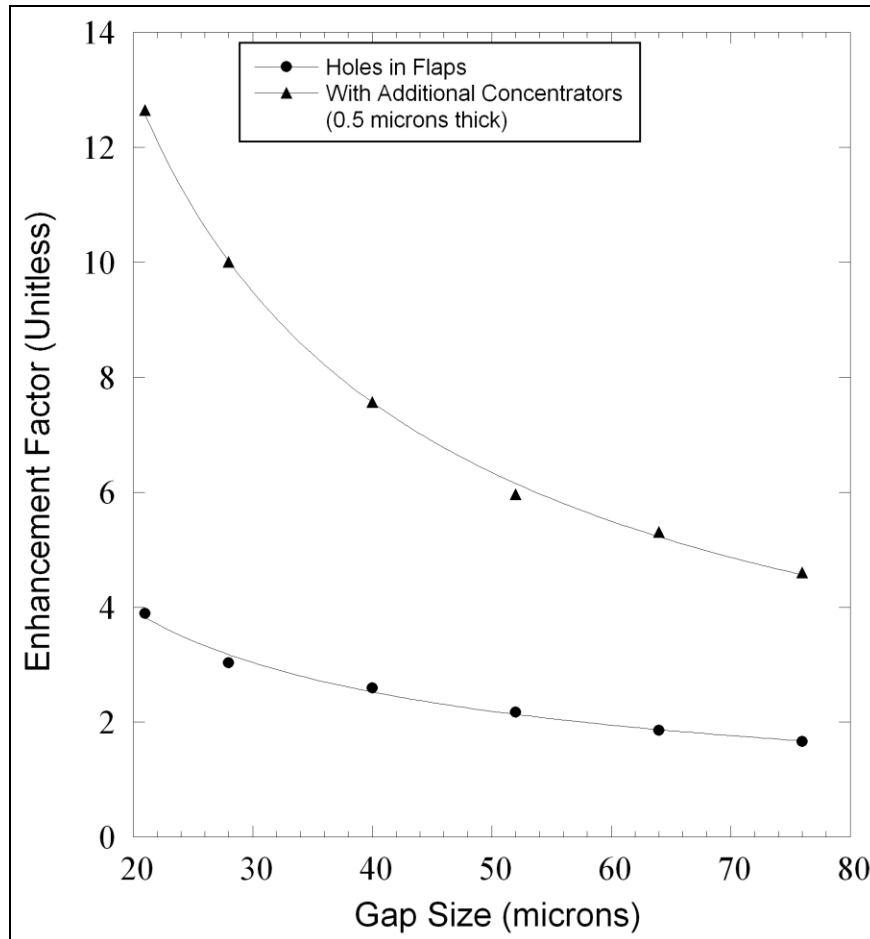


Figure 7. Enhancement curves demonstrating effect of the addition of a second pair of large, stationary flux concentrators.

3.3 Comb Drive, In-phase Flux Concentrators

Since the magnetic modeling indicated that the addition of stationary flux concentrators had little effect on the modulation, another fundamental change was made to the overall design. The main changes were (1) the air gap was decreased to 11 μm , (2) the size of the moving concentrators was increased, (3) the number and type of etch holes was increased, and (4) the moving concentrators were joined together by small struts to either side of the air gap (figure 8a). These changes allowed us to change the normal operation mode to an in-phase motion that would alternately enhance the field at the position of the sensor or *shunt* the field away from the sensor, thus increasing the percentage modulation. The flaps now had a height of 110 μm , a short side length of 80 μm , and a long side length of 308 μm . Smaller, diamond shaped etch holes were placed near the air gap to facilitate full release of the flaps. The flaps were modeled as solid, 0.25 μm thick permalloy and all nonmagnetic structural material was ignored (figure 8b). In order to simplify shunting, the position of the sensor remains roughly 4 μm above the moving flaps but is shifted laterally so as to be 16 μm away from the air gap edge of one of the flaps.

The enhancement curve was generated from the magnetic models and the corresponding modulation curve for the new in-phase motion is shown in figure 6. Equation 1 is still used to determine percentage modulation but now both H_{S1} and H_{SR} are reduced due to shunting and the sensors location relative to the flaps. We see that now only 12 μm of motion would result in nearly 350% modulation of the field at the position of the sensor.

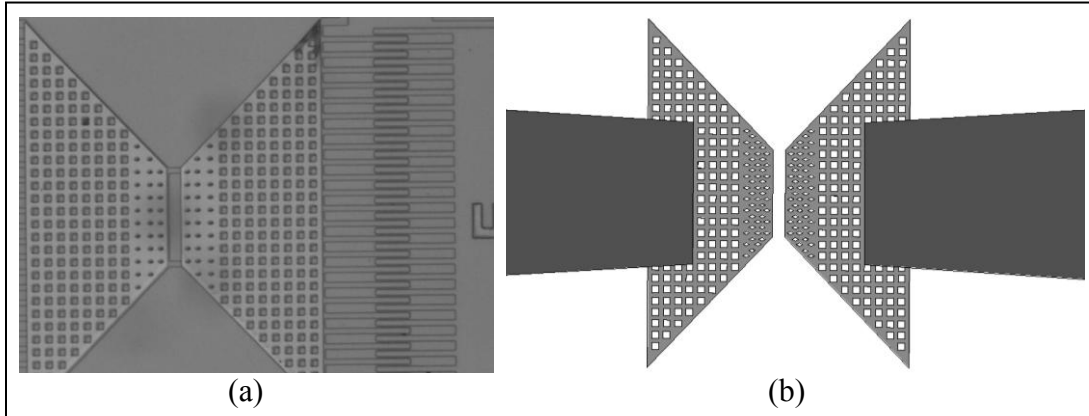


Figure 8. (a) Optical microscope image of the in-phase flux concentrator design and (b) the concentrators as drawn for modeling. The darker trapezoids are part of the stationary concentrators, the remainder being out of view.

The new location of the sensor necessitated us running additional models to determine if the flux environment around the sensor would create problems. Specifically, we were concerned with the flux line behavior around the release holes. As the flux lines will both flow around the holes and arc out above and below them (figure 9), we wanted to see if 5 μm above release holes would place the sensor in a noisy, turbulent flux environment. We see in figure 10 that the flux lines are indeed flowing around the release holes. The rectangular regions to either side of the flaps indicate a decrease in field lines because this plot shows field in the plane of the moving flaps and those regions are where the field is largely in the larger, stationary flaps that overlap the moving flaps (figure 8b). We were able to determine that the flux environment above the moving flaps is relatively smooth until one is 1 μm away from the flap surface (figure 11). Only then do the models indicate variations in the magnetic field strength due to the etch holes.

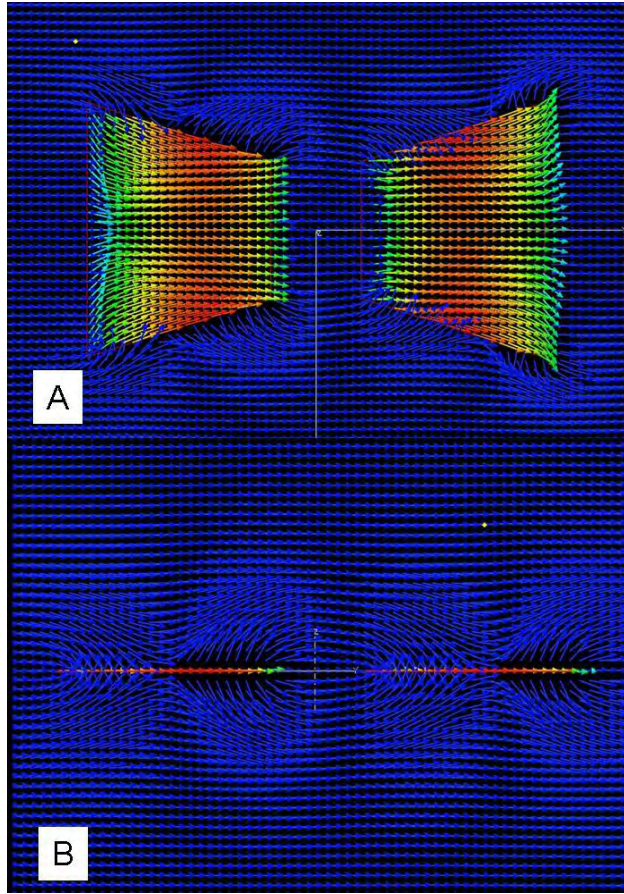


Figure 9. (a) Top view and (b) side view of magnetic flux lines around concentrators. Color from blue to red denotes low to high flux density, respectively.

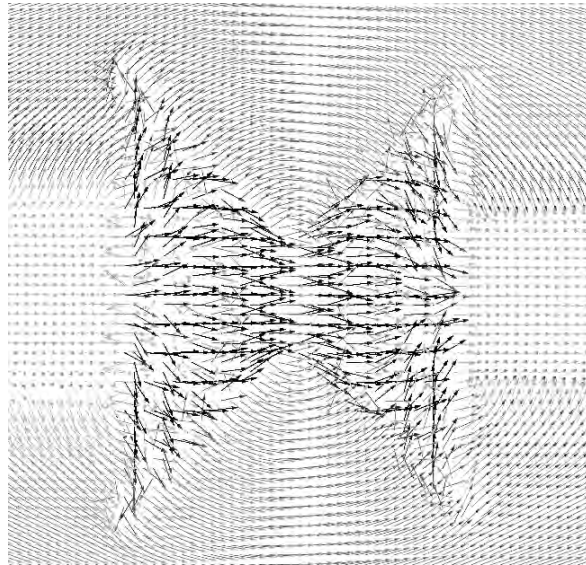


Figure 10. Flow of magnetic flux lines around etch holes in concentrators.

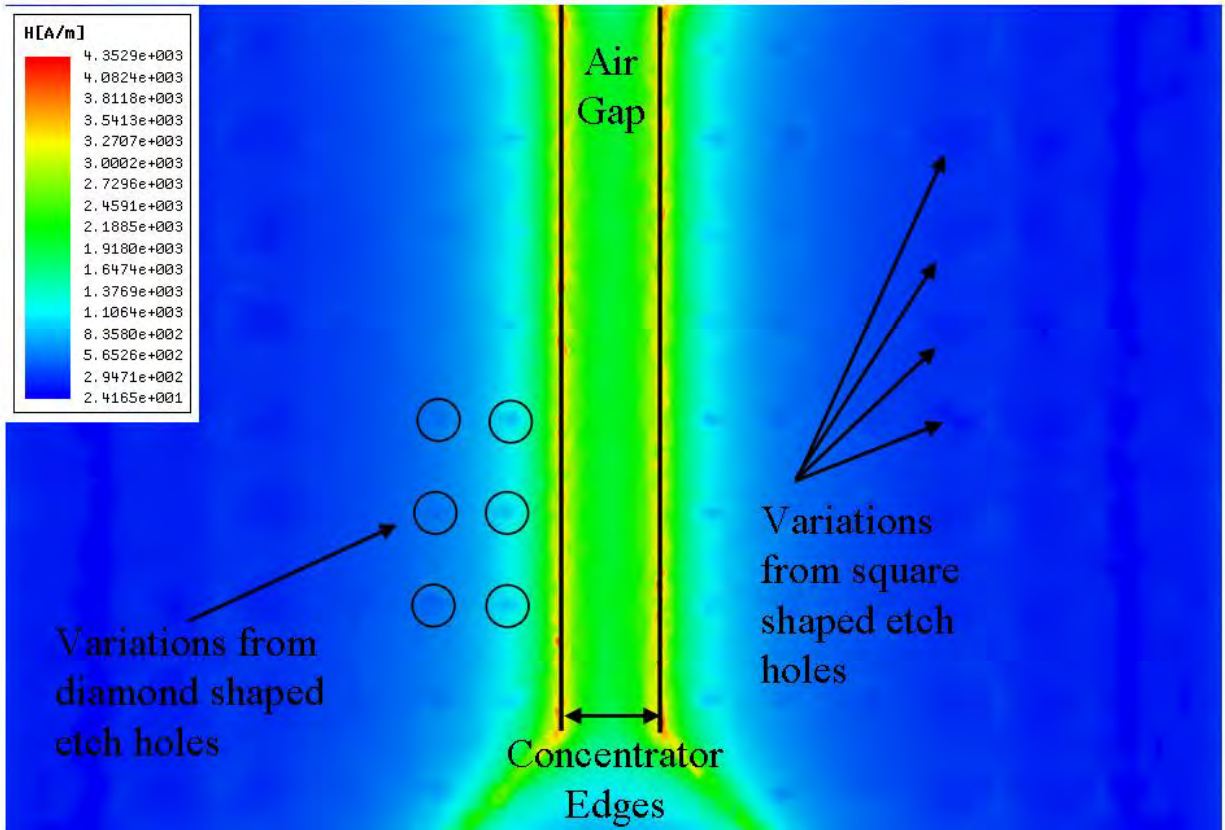


Figure 11. Variations in the magnetic field strength at 1 micron above concentrators due to etch holes.

4. Discussion and Conclusions

We have described the magnetic modeling that has facilitated the development of the MEMS flux concentrator, a device that uses magnetic flux concentrators deposited on MEMS structures that modulate low frequency signals at the position of a magnetic sensor. We presented magnetic modeling results of various designs, including our current design, focusing on key design elements. A comparison of measured magnetic field enhancement values to values calculated from magnetic modeling was presented and shown to agree to within 4%. Working devices have been packaged for testing. In figure 12, we see four of our devices ready for testing. The four etched windows allow us to verify motion of the devices as well as determine the resonant frequency of each device. As described in section 3.2, these devices are flip chip bonded with the MEMS devices on the bottom wafer piece and the magnetic sensing elements are on the top piece, centered over the gap of each pair of flux concentrators. Using this packing we have been able to confirm the concept of the MEMS flux concentrator (11).

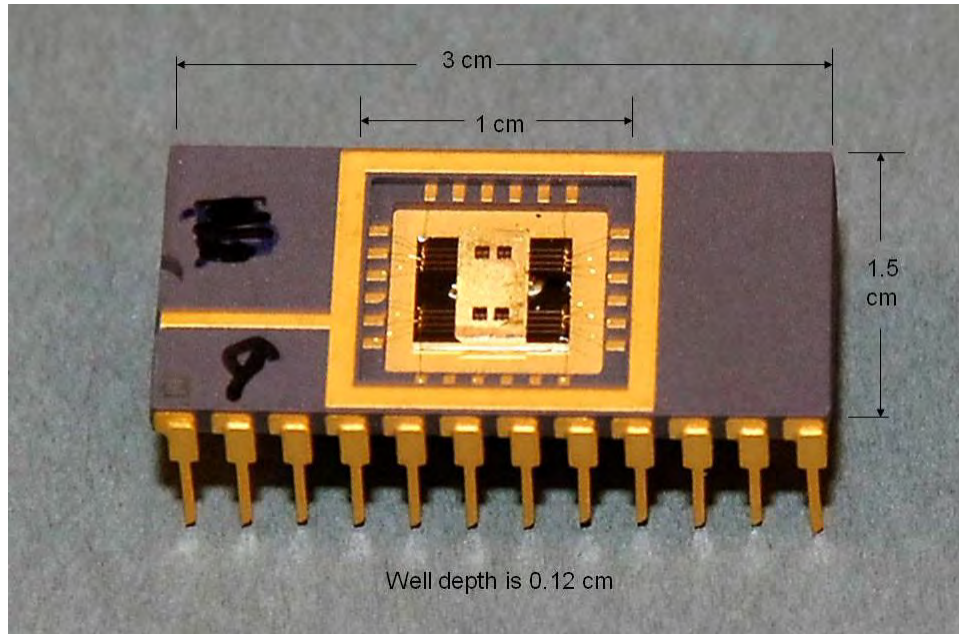


Figure 12. Four MEMs flux concentrator devices packaged for testing.

The use of macro-magnetic modeling has allowed us to gain insight in how design features impact magnetic flux lines, and achieve both high field enhancement and a large percentage field modulation. Work is continuing on the in-phase design and it is anticipated that vacuum packaging of the devices and the associated increase in Q , the resonant frequency divided by the frequency halfwidth of the resonant frequency, combined with the use of very sensitive magnetic tunnel junctions, will result in a detectivity of a few $\text{pT/Hz}^{1/2}$ at 1 Hz.

5. References

1. Guedes, A.; Almeida, J. M.; Cardoso, S.; Ferreira, R.; Freitas, P. P. Improving Magnetic Field Detection Limits of Spin Valve Sensors Using Magnetic Flux Guide Concentrators. *IEEE Trans. Magn.* **2007**, *43*, 2376–8.
2. Leroy, P.; Coillot, C.; Mosser, V.; Roux, A.; Chanteur, G. An ac/dc Magnetometer for Space Missions: Improvement of a Hall Sensor by the Magnetic Flux Concentration of the Magnetic Core of a Searchcoil. *Sens. Actuators A.* **2008**, *142*, 503–10.
3. Griffith, W. C.; Jimenez-Martinez, R.; Shah, V.; Knappe, S.; Kitching, J. Miniature Atomic Magnetometer Integrated with Flux Concentrators. *Appl. Phys. Lett.* **2009**, *94*, 023502–1.
4. Bondarenko, S. I.; Shablo, A. A.; Pavlov, P. P.; Perepelkin, S. S. Ferromagnetic Concentrator of a Magnetic Field for the Planar HTSC SQUID. *Physica C* **2002**, *372–376*, 158–61.
5. Brugger, S.; Simon, P.; Paul, O. Field Concentrator Based Resonant Magnetic Sensor. *IEEE Sensors 2006 EXCO*, Daegu, Korea, pp. 1016-9, 2006.
6. Chaves, R. C.; Freitas, P. P.; Ocker, B.; Maass, W. MgO Based Picotesla Field Sensors. *J. Appl. Phys.* **2008**, *103*, 07E931–1.
7. Leroy, P.; Coillot, C.; Roux, A. F.; Chanteur, G. M. High Magnetic Field Amplification for Improving the Sensitivity of Hall Sensors. *IEEE Sens. J.* **2006**, *6*, 707–13.
8. Brugger, S.; Paul, O. Magnetic Field Amplification by Slender Cuboid-shaped Magnetic Concentrators with a Single Gap. *Sens. Actuators A.* **2010**, *157*, 135–9.
9. Jiang, L.; Nowak, E. R.; Scott, P. E.; Johnson, J.; Slaughter, J. M.; Sun, J. J.; Dave, R. W. Low-frequency Magnetic and Resistance Noise in Magnetic Tunnel Junctions. *Phys. Rev. B* **2004**, *69*, 055407–1.
10. Stutzke, N. A.; Russek, S. E.; Pappas, D. P.; Tondra, M. Low-frequency Noise Measurements on Commercial Magnetoresistive Magnetic Field Sensors. *J. Appl. Phys.* **2005**, *97*, 10Q107.
11. Edelstein, A. S.; Burnette, J. E.; Fischer, G. A.; Olver, K.; Egeelhoff, Jr., Wm.; Nowak, E.; Cheng, Shu-Fan. Validation of the Microelectromechanical System Flux Concentrator Concept for Minimizing $1/f$ Noise. *J. Appl. Phys.* **2009**, *105*, 07E720.

12. Edelstein, A. S.; Fischer, G. A.; Pederson, M.; Nowak, E. R.; Cheng, Shu-Fan; Nordman, C. A. Progress Toward a Thousandfold Reduction in $1/f$ Noise in Magnetic Sensors using an ac Microelectromechanical System Flux Concentrator. *J. Appl. Phys.* **2006**, *99*, 08B317.

List of Symbols, Abbreviations, and Acronyms

3-D	three-dimensional
ARL	U.S. Army Research Laboratory
Cr	chromium
HF	hydrofluoric acid
MEMS	microelectromechanical system
MgO	magnesium oxide
MTJ	magnetic tunnel junctions
NiFE	nickel-iron
SQUIDs	superconducting quantum interference device

NO. OF COPIES	ORGANIZATION	NO. OF COPIES	ORGANIZATION
1 ELEC	ADMNSTR DEFNS TECHL INFO CTR ATTN DTIC OCP 8725 JOHN J KINGMAN RD STE 0944 FT BELVOIR VA 22060-6218	1	COMMANDER US ARMY RDECOM ATTN AMSRD AMR W C MCCORKLE 5400 FOWLER RD REDSTONE ARSENAL AL 35898-5000
1	DEFNS INTLLGNC AGCY ATTN RTS-2A TECHL LIB WASHINGTON DC 20301	1	NAV RSRCH LAB ATTN 5220 TECHL LIB 4555 OVERLOOK AVE SW WASHINGTON DC 20375-5320
1 CD	OFC OF THE SECY OF DEFNS ATTN ODDRE (R&AT) THE PENTAGON WASHINGTON DC 20301-3080	1	US GOVERNMENT PRINT OFF DEPOSITORY RECEIVING SECTION ATTN MAIL STOP IDAD J TATE 732 NORTH CAPITOL ST NW WASHINGTON DC 20402
1	US ARMY RSRCH DEV AND ENGRG CMND ARMAMENT RSRCH DEV & ENGRG CTR ARMAMENT ENGRG & TECHN LGY CTR ATTN AMSRD AAR AEF T J MATTS BLDG 305 ABERDEEN PROVING GROUND MD 21005-5001	1	THE JOHNS HOPKINS UNIV APPLD PHYSIC LAB ATTN TECHL LIB JOHNS HOPKINS RD LAUREL MD 20707
1	US ARMY ARDEC ATTN AMSRD AAR AEP S R T KINASEWITZ BLDG 353N PICATINNY ARSENAL NJ 07806-5000	1	SOUTHWEST RSRCH INST ATTN S CERWIN 6220 CALEBRA RD SAN ANTONIO TX 78238
1	US ARMY ARDEC ATTN AMSRD AAR EMK TECH LIB BLDG 59 PHIPPS RD PICATINNY ARSENAL NJ 07806-5000	18	US ARMY RSRCH LAB ATTN IMNE ALC HRR MAIL & RECORDS MGMT ATTN RDRL CI J PELLEGRINO ATTN RDRL CIO LL TECHL LIB ATTN RDRL CIO MT TECHL PUB ATTN RDRL SES J EICKE ATTN RDRL SES P A EDELSTEIN ATTN RDRL SES P G FISCHER (10 HCS) ATTN RDRL SES P J FINE ATTN RDRL SES P M SCANLON ADELPHI MD 20783-1197
1	US ARMY ARDEC ATTN AMSRD AAR HEP A A M HOHIL BLDG 407 PICATINNY ARSENAL NJ 07806-5000		
1	US ARMY INFO SYS ENGRG CMND ATTN AMSEL IE TD A RIVERA FT HUACHUCA AZ 85613-5300		

INTENTIONALLY LEFT BLANK.